ACS OMEGA

http://pubs.acs.org/journal/acsodf

Article

Density Functional Calculation of $H_2O/CO_2/CH_4$ for Oxygen-Containing Functional Groups in Coal Molecules

Dan Zhao and Xiaoqing Liu*

Cite This: *ACS Omega* 2022, 7, 17330−17338

Read Online

ACCESS | Metrics & More | Article Recommendations

ABSTRACT: To investigate the adsorption mechanism of H_2O, CO_2, and CH_4 molecules on oxygen-containing functional groups (OFGs) in coal molecules, quantum chemical density functional theory (DFT) simulations were performed to study the partial density of states and Mulliken bond layout of H_2O molecules bonded to different OFGs. The adsorption energy and Mulliken charge distribution of the H_2O, CO_2, and CH_4 molecules for each OFG were determined. The results showed that H_2O molecules form 2, 1, 1, and 1 hydrogen bonds with −COOH, −OH, —C═O, and −O−R groups, respectively. Double hydrogen bonds connected the H_2O molecules to −COOH with the smallest adsorption distances and highest Mulliken bond layout values, resulting in the strongest bonding between the H_2O molecules and −COOH. The most stable configuration for the adsorption of these molecules by the −OH group was when the O−H bond in the OFG served as a hydrogen bond donor and the O atom in the H_2O molecule served as a hydrogen bond acceptor. The order of the bonding strength between the OFGs and H_2O molecules was Ph−COOH > Ph−OH > Ph—C═O > Ph−O−R. The adsorption energy calculation results showed that H_2O molecules have a higher adsorption stability than CO_2 and CH_4 molecules. Compared with the −OH, —C═O, and −O−R groups, the −COOH group had a higher adsorption capacity for H_2O, CO_2, and CH_4 molecules. The adsorption stability of the CO_2 molecules for each OFG was higher than that of the CH_4 molecules. From the Mulliken charge layout, it was clear that after the adsorption of the H_2O molecules onto the OFGs, the O atoms in the OFGs tend to gain electrons, while the H atoms involved in bonding with the H_2O molecules tend to lose electrons. The formation of hydrogen bonds weakens the strength of the bonds in the H_2O molecule and OFGs, and thus, the bond lengths were elongated.

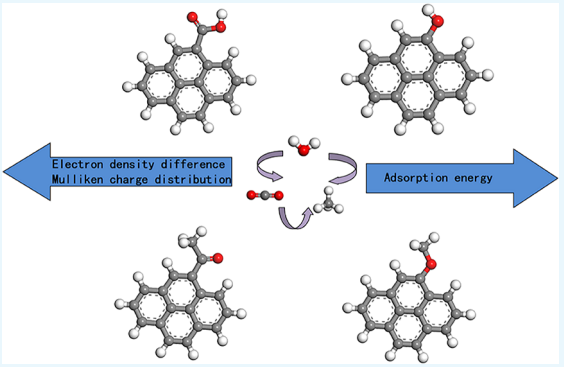

1. INTRODUCTION

The continuous exploitation of coal, oil, and natural gas could lead to the exhaustion of fossil-based energy sources. Fossil fuel usage is associated with the release of large amounts of greenhouse gases, such as CO_2 and CH_4, which threaten the ecological environment. Therefore, the development of cleaner, nonconventional energy sources is the way forward. Coal bed methane (CBM) is a gas resource that is associated and symbiotic with coal. It is a clean, high-quality energy source (compared to coal) and a chemical raw material with CH_4 as the main component while containing certain amounts of CO_2 and N_2,[1] with largely no pollutants after combustion (assuming CO_2 as a non-pollutant). Hence, CBM can be used as a clean energy source to improve the energy mix.[2−5] The CO_2 emitted from the production processes and purified by adsorption, membrane separation, absorption, and low-temperature separation is injected into a coal seam to induce a competitive adsorption between CO_2 and CH_4, thereby effectively displacing CH_4 gas in the coal seam and realizing enhanced coal bed methane (ECBM) recovery. CO_2 carbon capture, utilization, and storage (CCUS) and CH_4 separation and utilization are feasible and effective ways to reduce the greenhouse effect. Hence, it is important to study the adsorption properties of CO_2 on coal surfaces to reduce greenhouse gas emissions.[6]

The adsorption of gases on the surface of coal seams is influenced by the pressure,[7] temperature,[8] moisture content,[9−11] surface functional groups,[12−14] pore structure,[15,16] and degree of coalification of the coal matrix,[17−19] among which the surface functional groups have a particularly important influence in the case of medium and low-rank coals. In recent years, the density functional theory (DFT) and molecular dynamics (MD) simulations, as well as improvements made to computer hardware, have made quantum

Received: March 3, 2022
Accepted: April 28, 2022
Published: May 9, 2022

theory and molecular simulation methods effective theoretical tools for studying the adsorption properties of gases in coal seams and for calculating surface interactions.[20−23] Huo et al. investigated the adsorption strength of different oxygen-containing functional groups (OFGs) for H_2O molecules using the DFT, and based on the analysis of the electron density and potential energy density, the order of the capacity of four different OFGs to adsorb H_2O molecules was found to be Ph−C−O−OH > Ph−COOH > Ph−OH > Ph−CHO.[24] Wang et al. studied the interaction between H_2O molecules and OFGs using the quantum chemical DFT and concluded that the order of influence of the H_2O molecules on the adsorption stability of the OFGs was carboxyl group > phenolic hydroxyl group > aldehyde group > ether and that the OFGs could improve the wettability on the surface of coal molecules.[25] Xiang et al. investigated the adsorption behavior of the binary component CH_4:CO_2 (molar ratio of 1:1) using the grand canonical Monte Carlo (GCMC) method, and the results showed that the adsorption capacity for CO_2 was significantly greater than that for CH_4 at the same temperature and pressure, the competitive advantage was evident, and CO_2 injection could help effectively displace CH_4.[26] Xu et al. investigated the adsorption and desorption of CH_4 and CO_2 on a 4 × 4 carbon model using the DFT, and the results showed that CO_2 had a higher adsorption stability than CH_4 and that CO_2 injection could promote the desorption of CH_4.[27] Zhou et al. used the quantum chemical DFT to study the interaction between CH_4 and H_2O on the surface of different grades of coal and concluded that a coal−H_2O system has a greater adsorption energy than a coal−CH_4 system for coals of different maturities and that water injection could improve CBM recovery.[28] Yu et al. calculated the competitive adsorption and self-diffusion of CH_4, CO_2, and H_2O on the surface of low-rank coal vitrinite ($C_{214}H_{180}O_{24}N_2$) using GCMC and MD simulations.[29] The results showed that in the $CH_4/CO_2/H_2O$ = 1:1:1 ternary competitive system, the adsorption amount of the mirror mass group at the same temperature and pressure was in the order of H_2O > CO_2 > CH_4, and the value of the self-diffusion coefficient was in the order of D_{H2O} > D_{CO2} > D_{CH4} in the saturated adsorption configuration. This shows that the adsorption capacity is highest for H_2O molecules and that injecting water into a coal seam can help improve CBM production. The adsorption effect of H_2O was better than that of CO_2, which could accelerate the recovery of coal seam gas.[29]

Many simulations and calculations have been performed on the adsorption of H_2O, CO_2, CH_4, and other molecules on the surface of coal molecules;[30−33] however, few studies have analyzed the adsorption of small molecules at the atomic and electronic levels. To investigate the adsorption behavior of small molecules of H_2O, CO_2, and CH_4 on different OFGs (−COOH, −OH, —C═O, and −O−R) in the coal molecules, this study analyzed and compared the interactions between these molecules and each OFG on the surface of a coal model based on the DFT. Moreover, the adsorption mechanism was explored to provide a reference for studying the gas adsorption characteristics on the surface of coal molecules containing different OFGs and to provide theoretical support for the application of H_2O-ECBM and CO_2-ECBM.

2. CALCULATION METHOD

The optimization of the molecular models of OFGs, H_2O, CO_2, and CH_4 and the calculation of the molecular properties in this study were conducted using the DS BIOVIA Materials Studio 2020 software. The geometric optimization of OFGs, H_2O, CO_2, and CH_4 molecules and the calculation of the adsorption energy of small molecules in OFGs were done using the Dmol^3 module. The maximum iteration for the geometric optimization was set to 500 to ensure convergence. The correlation function adopted for the electron exchange was the Perdew−Burke−Ernzerhof (PBE) functional based on generalized gradient approximation (GGA),[34] the Grimme method was used for the DFT-D correction, DFT Semicore Pseudopots and double numeric with polarization basis set (DNP) was employed,[35] the accuracy was set to Fine, unrestricted electron spins were considered, and symmetry was applied. The convergence accuracy of the self-consistent field was set to 1.0×10^{-6},[36] the maximum number of SCF cycles was set to 500, and the smearing value was set to 0.005 Å. An energy value of 1.0×10^{-5} Ha was set as the convergence criterion for the geometric optimization. The maximum force was set to 0.002 Ha/Å, and the maximum displacement was set to 0.005 Å.

The energy of the completely optimized stable adsorption configuration was optimized using the CASTEP module to calculate its partial density of states (PDOS),[37] Mulliken bond layout, and electron density difference. Different stable adsorption configurations were optimized in periodic unit cells of 15 Å × 15 Å × 15 Å. The exchange correlation function and convergence standard were the same as those employed in the Dmol^3 module, and ultra-soft pseudopotentials were used to describe the interaction between the electrons and ions.[38] The smearing value used for the PDOS analysis was 0.2 eV. The electron density difference was calculated by defining the density difference for the H_2O, CO_2, and CH_4 molecules in different adsorption configurations by Edit Sets, and the electron density difference graph was derived using Analysis.

The adsorption stability of the H_2O, CO_2, and CH_4 molecules on different OFG surfaces can be expressed in terms of the adsorption energy. If the adsorption energy is negative, the reaction is exothermic. The lower the value, the stronger and more stable the adsorption, and vice versa. The calculation formula for the adsorption energy is as follows:

$$E_{ads} = E_{A/B} - E_A - E_B \quad (1)$$

where E_{ads} is the adsorption energy of each molecule on different OFG surfaces (kJ/mol); $E_{A/B}$ is the total energy of different OFGs with each small molecule after adsorption (kJ/mol); E_A is the energy of different OFGs (kJ/mol); and E_B is the energy of different small molecules (H_2O, CO_2, and CH_4) (kJ/mol).

To comprehensively analyze the effect of the OFGs in the coal molecules on the adsorption of H_2O, CO_2, and CH_4 molecules, 2 × 2 hexacyclic aromatic clusters ($C_{16}H_{10}$) were selected to simulate the surface of coal molecules during the quantum chemical calculations.[39] The interactions between the OFGs, such as carboxyl (Ph−COOH), phenolic hydroxyl (Ph−OH), carbonyl (Ph—C═O), and ether (Ph−O−R) groups and the different molecules were calculated separately (where Ph− denotes phenyl, and R− denotes alkyl).

https://doi.org/10.1021/acsomega.2c01278
ACS Omega 2022, 7, 17330−17338

3. RESULTS AND DISCUSSION

3.1. Hydrogen Bond Analysis. The most stable configuration of H_2O molecules for adsorption by different OFGs was used as an example to analyze the bonding properties. Figure 1 shows four adsorption configurations. As shown in Figure 1, the most stable adsorption positions of the H_2O molecules on the different OFGs are all above the OFG, and the initial configurations of the H_2O molecules are in the down form, except for the H_2O molecules at Ph−O−R, which are in the up form. The H_2O molecule forms 2, 1, 1, and 1 hydrogen bonds with −COOH, −OH, —C═O, and −O−R, respectively. The H_2O molecule forms a double hydrogen bond when adsorbed by −COOH with the shortest hydrogen bond length of 1.700 Å. In the adsorption by the −OH group, the O−H bond in the OFG as the hydrogen bond donor and the O atom in the H_2O molecule as the hydrogen bond acceptor are the most stable adsorption configuration, with a hydrogen bond length of 1.841 Å. In the adsorption by the —C═O and −O−R groups, the hydrogen bond lengths formed are 1.877 and 2.048 Å, respectively. The initial bond length of the H_2O molecule is 0.970 Å, and the initial bond angle is 103.749°. Table 1 presents the bond lengths and bond angles of the H_2O molecules at different OFG adsorption equilibria. Table 2 presents the bond lengths of the OFGs before and after the adsorption equilibria.

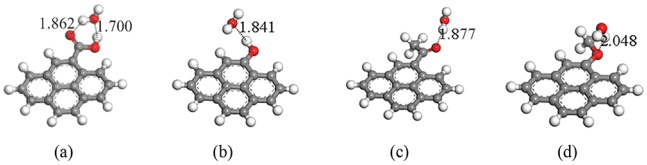

Figure 1. The most stable configurations of H_2O molecules for adsorption by different OFGs (white: H atoms; red: O atoms; gray: C atoms). (a) H_2O/Ph−COOH, (b) H_2O/Ph−OH, (c) H_2O/Ph—C═O, and (d) H_2O/Ph−O−R.

Table 1. Bond Length and Bond Angle of H_2O Molecules for Adsorption by Different OFGs at Adsorption Equilibrium[a]

adsorption site	$d(H_{W1},O_W)$/Å	$d(O_W,H_{W2})$/Å	$\theta(H_{W1}O_WH_{W2})$/(°)
Ph−COOH	0.992	0.971	104.957
Ph−OH	0.975	0.972	104.683
Ph—C═O	0.983	0.969	104.277
Ph−O−R	0.974	0.970	102.946

[a]H_W and O_W denote the H and O atoms in the H_2O molecule, respectively, H_{W1} is the H atom involved in bonding with the H_2O molecule, H_{W2} is the H atom not involved in bonding with the H_2O molecule, and neither H atom is involved in bonding with the H_2O molecule and Ph−OH.

The bonding mechanism of the H_2O molecules with each OFG was further elucidated by calculating the PDOS. Figure 2a,b shows the PDOS of the H_2O molecule forming two hydrogen bonds with the Ph−COOH surface. Figure 2a,b shows the hydrogen bonds $H_{W1}\cdots O_{S1}$ between the H atom of the H_2O molecule and the O atom of the C═O bond in −COOH and the hydrogen bonds $H_S\cdots O_W$ between the H atom of the O−H bond in −COOH and the O atom of the H_2O molecule, respectively. The orbitals of O_{S1} and O_W are mainly distributed in the valence band near the Fermi energy level, and the distribution is not evident in the conduction band, which is favorable for bonding. In Figure 2a,b, the H 1s orbital and O 2p orbital are bonded in the energy range of −9 to −3 eV, and the anti-bonds are bonded in the energy range of 4−13 eV, with evident resonance phenomena, indicating the formation of two hydrogen bonds on the surface of the H_2O molecules and Ph−COOH. Hydrogen bonds are formed by the interaction between the H 1s orbital and O 2p orbital. The hydrogen bond $H_S\cdots O_W$ is stronger than $H_{W1}\cdots O_{S1}$ owing to the stronger delocalization of H 1s in Figure 2b than in Figure 2a. Figure 2c−e shows that the −9 to −3 eV, H 1s orbital, and O 2p orbital are bonded and that the 4−13 eV, H 1 s orbital, and O 2p orbital are anti-bonded. Corresponding to the hydrogen bond $H_S\cdots O_W$ between the H atom of the −OH group and the O atom in the H_2O molecule, the hydrogen bond $H_{W1}\cdots O_S$ between the H atom of the H_2O molecule and the O atom in the —C═O group and the hydrogen bond $H_{W1}\cdots O_S$ between the H atom of the H_2O molecule and the O atom in the −O−R group. From the off-domain nature of H 1s, as shown in Figure 2, it is clear that the order of the bonding strength between the OFGs and H_2O molecules is Ph−COOH > Ph−OH > Ph—C═O > Ph−O−R.

To quantify the bond strength of the H_2O molecules at different OFG sites, the Mulliken bond layout of the H_2O molecules adsorbed on the surfaces of different coal models was determined. Table 3 presents the results. Based on the calculation results, the average bond lengths of the H_2O molecules forming hydrogen bonds with different OFGs are 1.781, 1.841, 1.877, and 2.048 Å. The adsorption equilibrium distances are significantly lower than 3 Å, which is not near the covalent bond length (van der Waals forces act in the range of 3−5 Å). This shows that the adsorption mechanism of H_2O molecules on the OFGs is chemisorption. The Mulliken bond layouts of the H_2O molecules adsorbed at different OFG sites are in the order of Ph−COOH > Ph−OH > Ph—C═O >

Table 2. Bond Length of OFGs before and after Adsorption Equilibrium[a]

adsorption site	atomic relationship	d(before adsorption)/Å	d(after adsorption)/Å
Ph−COOH	$C{=}O_{S1}$	1.223	1.239
	$C{-}O_{S2}$	1.369	1.344
	O_{S2}−Hs	0.980	1.012
Ph−OH	$C{-}O_S$	1.373	1.362
	$O_S{-}H_S$	0.973	0.989
Ph—C═O	$C{=}O_S$	1.231	1.238
Ph−O−R	$Ph(C){-}O_S$	1.368	1.374
	$O_S{-}C(R)$	1.428	1.435

[a]H_S and O_S denote the H and O atoms of the OFG, respectively; O_{S1}: the O atom of the C═O bond in −COOH; O_{S2}: the O atom of the O−H bond in −COOH.

https://doi.org/10.1021/acsomega.2c01278
ACS Omega 2022, 7, 17330−17338

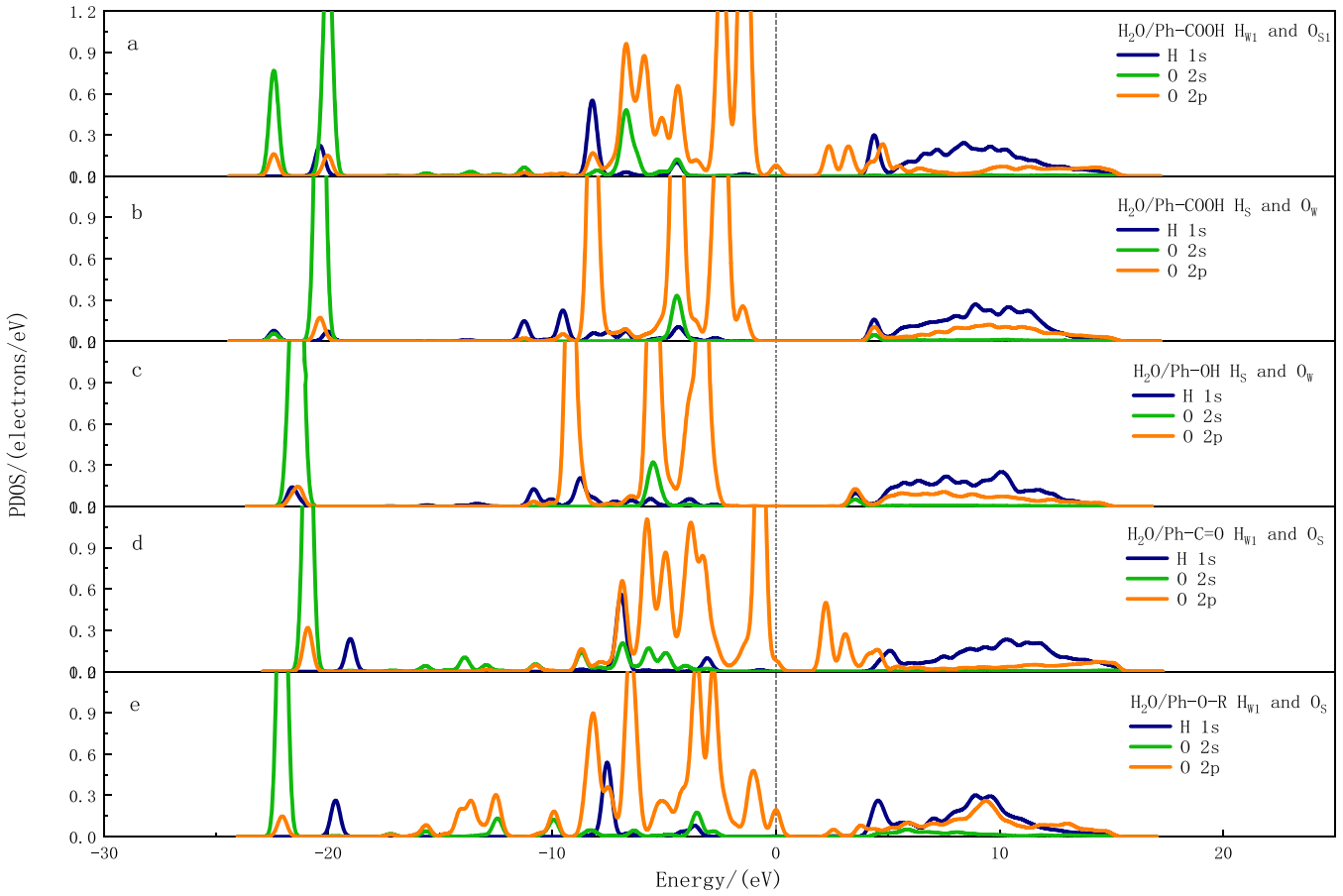

Figure 2. PDOS of hydrogen bond formation between H_2O molecules and each OFG. (a) H_2O/Ph−COOH, between H_{W1} and O_{S1}, (b) H_2O/Ph−COOH, between H_S and O_W, (c) H_2O/Ph−OH, between H_S and O_W, (d) H_2O/Ph—C═O, between H_{W1} and O_S, and (e) H_2O/Ph−O−R, between H_{W1} and O_S.

Table 3. Mulliken Bond Layout of H_2O Molecules Adsorbed on the Surface of Different Coal Models[a]

adsorption configuration	H_2O/Ph−COOH		H_2O/Ph−OH	H_2O/Ph—C═O	H_2O/Ph−O−R
bond	$H_{W1}\cdots O_{S1}$	$H_S\cdots O_W$	$H_S\cdots O_W$	$H_{W1}\cdots O_S$	$H_{W1}\cdots O_S$
distance/Å	1.862	1.700	1.841	1.877	2.048
Mulliken layout	0.08	0.11	0.08	0.07	0.03

[a]H_W and O_W denote the H and O atoms in the H_2O molecule, H_S and O_S denote the H and O atoms of the OFG, respectively, and ··· represents the existence of hydrogen bonds between the two atoms.

Ph−O−R. The shorter the hydrogen bond length, the greater the Mulliken bond layout value, indicating stronger hydrogen bonds, a result consistent with the PDOS calculations of the hydrogen bond formation.

3.2. Adsorption Energy Calculation. Figure 3 shows the most stable adsorption configurations of the H_2O, CO_2, and CH_4 molecules for different OFGs. Table 4 shows the adsorption energies of the H_2O, CO_2, and CH_4 molecules for the OFGs. The results showed that the adsorption energies of the H_2O molecules for each OFG are significantly lower than those of the CO_2 and CH_4 molecules. The adsorption capacity is much greater than those of the CO_2 and CH_4 molecules; this is mainly attributed to the interaction between the H_2O molecules and each OFG via hydrogen bonding. The order of the strong and weak adsorption abilities of the H_2O molecules for different OFGs is Ph−COOH > Ph−OH > Ph—C═O > Ph−O−R. This order is in full agreement with the Mulliken bond layout order described above and also with the order of strong and weak adsorption capacity in the literature of Xia et al. and Gao et al.[40−42] The adsorption capacity of the H_2O molecules for Ph−COOH is much greater than that for the other OFGs because of the formation of double hydrogen bonds during the adsorption of the H_2O molecules by Ph−COOH, with an adsorption energy of −70.474 kJ/mol, which is close to the adsorption energy of −69.250 kJ/mol obtained by Xia et al.[40] Gao et al. calculated the adsorption energy between a single H_2O molecule and the hydroxyl, carbonyl groups in lignite as −43.140 and − 38.240 kJ/mol, respectively, which is closer to the results calculated in this paper.[41,42]

Both CO_2 and CH_4 are nonpolar molecules; however, CO_2 molecules have a strong polarizability and quadrupole moment, enabling them to easily interact with polar OFGs and exhibit significant electron transfer. The CH_4 molecule is an orthotetrahedral structure formed by averaging the energy and spatial orientation of one 2s orbital and three 2p orbitals; this structure is very stable and has less electron transfer when interacting with OFGs. The adsorption energy calculations of CO_2 and CH_4 molecules for each OFG show that the CO_2 molecules have a higher adsorption capacity than the CH_4 molecules. The order of the strong and weak adsorption capacities of the CO_2 molecules is Ph−COOH > Ph—C═O > Ph−OH > Ph−O−R, and the results are in agreement with

https://doi.org/10.1021/acsomega.2c01278
ACS Omega 2022, 7, 17330−17338

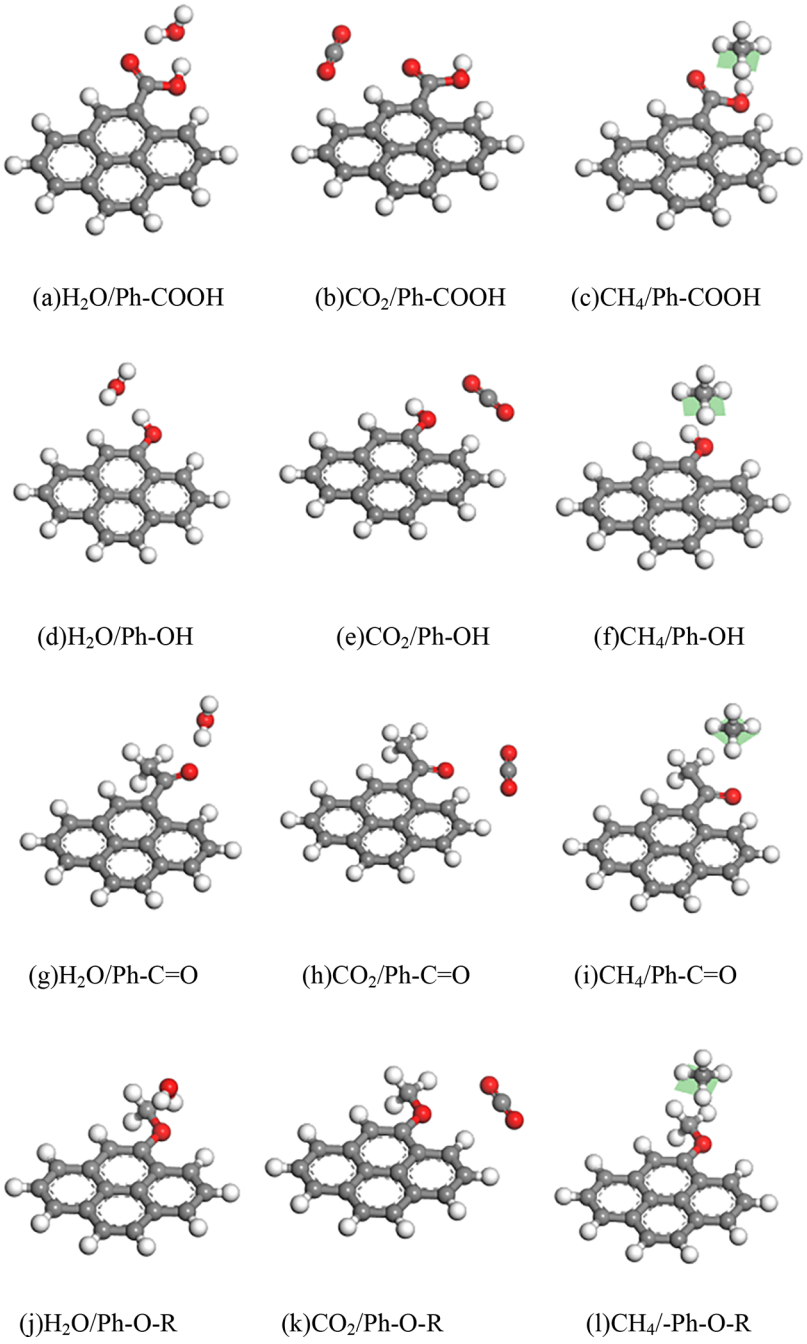

Figure 3. Most stable adsorption configurations of H_2O, CO_2, and CH_4 molecules for different OFGs (white: H atom; red: O atom; gray: C atom).

Table 4. Adsorption Energies of H_2O, CO_2, and CH_4 Molecules for Different OFGs

	adsorption energy/E_{ads} (kJ·mol^{-1})		
adsorption site	H_2O	CO_2	CH_4
Ph−COOH	−70.474	−13.437	−10.142
Ph−OH	−49.089	−12.259	−8.197
Ph—C═O	−40.997	−12.954	−7.123
Ph−O−R	−32.344	−10.681	−7.391

those obtained by Cheng et al.[43] The order of the strong and weak adsorption abilities of the CH_4 molecules is Ph−COOH > Ph−OH > Ph−O−R > Ph—C═O. Comparing the adsorption energy magnitudes of the different molecules for each OFG, it can be found that the adsorption energy values of H_2O, CO_2, and CH_4 molecules, particularly H_2O molecules, for −COOH were lower than those for the other OFGs, indicating that the adsorption ability is stronger on the −COOH group.

3.3. Charge Analysis. The variation in the charge between the bonding atoms or interacting atoms when H_2O, CO_2, and CH_4 molecules were adsorbed on different OFG surfaces can be graphically represented by electron density difference diagrams. The charge transfer of different molecules adsorbed on each OFG surface can be represented visually using the Mulliken charge layout. Figure 4 shows the electron density difference diagrams of the H_2O, CO_2, and CH_4 molecules in each OFG adsorption system. In the figure, the negative value (blue area) indicates a decrease in the electron density before relative adsorption, and the darker the color, the greater the

https://doi.org/10.1021/acsomega.2c01278
ACS Omega 2022, 7, 17330−17338

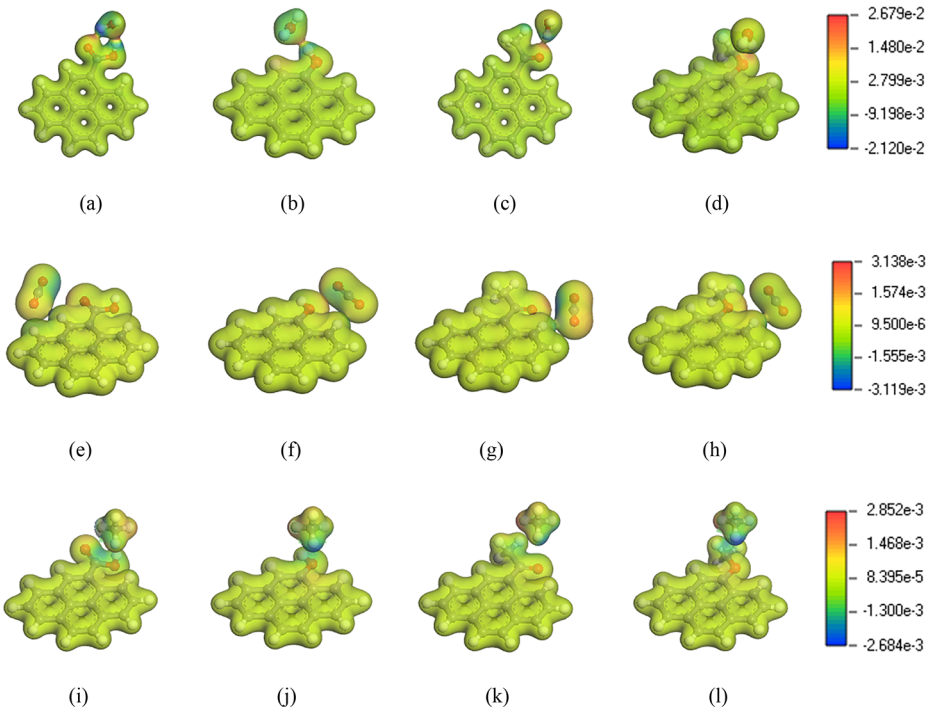

Figure 4. Electron density difference diagrams of H_2O, CO_2, and CH4 molecules in different OFG adsorption systems: (a) H_2O/Ph−COOH, (b) H_2O/Ph−OH, (c) H_2O/Ph—C═O, (d) H_2O/Ph−O−R, (e) CO_2/Ph−COOH, (f) CO_2/Ph−OH, (g) CO_2/Ph—C═O, (h) CO_2/Ph−O−R, (i)CH_4/Ph−COOH, (j) CH_4/Ph−OH, (k) CH_4/Ph—C═O, and (l) CH_4/Ph−O−R.

Table 5. Mulliken Charge Layout of H_2O Molecules for Different OFGs before and after Adsorption Equilibrium

adsorption site	atom	Mulliken (before adsorption)	Mulliken (after adsorption)	Mulliken (variance)	atom	Mulliken (before adsorption)	Mulliken (after adsorption)	Mulliken (variance)
Ph−COOH	H_S	0.274	0.314	0.040	O_W	−0.499	−0.538	−0.039
	O_{S2}	−0.434	−0.454	−0.020	H_{W1}	0.249	0.307	0.058
	O_{S1}	−0.427	−0.492	−0.065	H_{W2}	0.249	0.267	0.018
	C	0.474	0.484	0.010				
Ph−OH	H_S	0.263	0.295	0.032	O_W	−0.499	−0.512	−0.013
	O_S	−0.441	−0.469	−0.028	H_{W1}	0.249	0.273	0.024
	C	0.287	0.280	−0.007	H_{W2}	0.249	0.277	0.028
Ph—C═O	O_S	−0.398	−0.441	−0.043	H_{W1}	0.249	0.292	0.043
	C	0.296	0.309	0.013	O_W	−0.499	−0.563	−0.064
	-				H_{W2}	0.249	0.244	−0.005
Ph−O−R	O_S	−0.462	−0.493	−0.031	H_{W1}	0.249	0.287	0.038
	Ph(C)	0.295	0.282	−0.013	O_W	−0.499	−0.547	−0.048
	R(C)	0.013	−0.001	−0.014	H_{W2}	0.249	0.254	0.005

decrease in the electron density; the positive value (red area) indicates an increase in the electron density before relative adsorption, and the darker the color, the greater the increase in the electron density. To clearly observe the electron density difference diagrams, the isosurface value for the H_2O and CH_4 molecules adsorbed on the OFG surface in the stable configuration was taken as 0.20 electron/Å^3, and the isosurface value for the CO_2 molecules adsorbed on the OFG surface in the stable configuration was taken as 0.05 electron/Å^3. Tables 5−7 present the Mulliken charge layouts of the H_2O, CO_2, and CH_4 molecules adsorbed on different OFG surfaces before and after adsorption equilibrium, respectively.

From Figure 4a−d and Table 5, it can be seen that the O−H bond in −COOH acts as a hydrogen bond donor and the O atom in the H_2O molecule acts as a hydrogen bond acceptor; after adsorption, the H atom in −COOH loses 0.040 electrons, while the O atom in the H_2O molecule gains 0.039 electrons. The O−H bond in the H_2O molecule acts as a hydrogen bond donor, and the O atom in the C═O bond of −COOH acts as a hydrogen bond acceptor. After adsorption, the H atom in the H_2O molecule loses 0.058 electrons, and the O atom in the C═O bond of −COOH gains 0.065 electrons, consistent with the electron density difference diagrams. In addition to the O atom in the C═O bond of COOH, the O atom in the O−H bond also gains electrons because of the strong electronegativity of the O atom on the OFG, which easily gains electrons, and the H atom in the H_2O molecule is the main electron-losing atom. The formation of hydrogen bonds weakens the bonding strength between the H_2O molecule and OFG. From Tables 1 and 2, it can be seen that d(C═O_{S1}), d(O_{S2}−Hs), and d(H_{W1},O_W) in the H_2O/Ph−COOH stable adsorption configuration elongate by 0.016, 0.032, and 0.022 Å, respectively, similar to the C═O bond and O−H bond elongation distances calculated by Gao et al.,[44] and the

https://doi.org/10.1021/acsomega.2c01278
ACS Omega 2022, 7, 17330−17338

Table 6. Mulliken Charge Layout of CO_2 Molecules for Different OFGs before and after Adsorption Equilibrium[a]

adsorption site	atom	Mulliken (before adsorption)	Mulliken (after adsorption)	Mulliken (variance)	atom	Mulliken (before adsorption)	Mulliken (after adsorption)	Mulliken (variance)
Ph−COOH	C	0.474	0.473	−0.001	C_W	0.553	0.569	0.016
	O_{S1}	−0.427	−0.438	−0.011	O_{W1}	−0.276	−0.267	0.009
	O_{S2}	−0.434	−0.432	0.002	O_{W2}	−0.276	−0.297	−0.021
	H_S	0.274	0.274	0				
Ph−OH	O_S	−0.441	−0.458	−0.017	C_W	0.553	0.579	0.026
	H_S	0.263	0.269	0.006	O_{W1}	−0.276	−0.290	−0.014
					O_{W2}	−0.276	−0.289	−0.013
Ph—C═O	O_S	−0.398	−0.408	−0.010	C_W	0.553	0.573	0.020
	C	0.296	0.294	−0.002	O_{W1}	−0.276	−0.276	0
					O_{W2}	−0.276	−0.300	−0.024
Ph−O−R	O_S	−0.462	−0.472	−0.010	C_W	0.553	0.573	0.020
	Ph(C)	0.295	0.294	−0.001	O_{W1}	−0.276	−0.282	−0.006
	R(C)	0.013	0.001	−0.012	O_{W2}	−0.276	−0.286	−0.010

[a]C_W: the C atom in CO_2 molecule; O_{W1}, O_{W2}: two O atoms in CO_2 molecule.

Table 7. Mulliken Charge Layout of CH_4 Molecules for Different OFGs before and after Adsorption Equilibrium[a]

adsorption site	atom	Mulliken (before adsorption)	Mulliken (after adsorption)	Mulliken (variance)	atom	Mulliken (before adsorption)	Mulliken (after adsorption)	Mulliken (variance)
Ph−COOH	C	0.474	0.467	−0.007	C_{W1}	−0.314	−0.342	−0.028
	O_{S1}	−0.427	−0.428	−0.001	H_T	0.316	0.338	0.022
	O_{S2}	−0.434	−0.425	0.009				
	H_S	0.274	0.274	0				
Ph−OH	O_S	−0.441	−0.439	0.002	C_{W1}	−0.314	−0.326	−0.012
	H_S	0.263	0.262	−0.001	H_T	0.316	0.323	0.007
Ph—C═O	O_S	−0.398	−0.398	0	C_{W1}	−0.314	−0.323	−0.009
	C	0.296	0.297	0.001	H_T	0.316	0.321	0.005
Ph−O−R	O_S	−0.462	−0.461	0.001	C_{W1}	−0.314	−0.323	−0.009
	Ph(C)	0.295	0.295	0	H_T	0.316	0.327	0.011
	R(C)	0.013	0.004	−0.009				

[a]C_{W1}: the C atom in the CH_4 molecule; H_T: all H atoms in the CH_4 molecule.

action of O_{S1} on H_{W1} changes the bond angle of the H_2O molecule from 103.749 to 104.957°. At the −OH site, the −OH functional group has an electron conjugation effect, leading to an increase in the density of the Π electron cloud on the benzene ring and a gain of 0.007 electrons. The O−H bond in Ph−OH acts as a hydrogen bond donor, and the O atom in the H_2O molecule acts as a hydrogen bond acceptor. After adsorption, the H atom in the O−H bond loses 0.032 electrons, the O atom gains 0.028 electrons, and the O atom in the H_2O molecule gains 0.013 electrons. In the H_2O/Ph−OH stable adsorption configuration, $d(O_S,H_S)$ and $d(H_{W1},O_W)$ elongate by 0.016 and 0.005 Å, respectively. The charge of the O atom in the H_2O molecule changes less, whereas the charges of the two H atoms in the H_2O molecule change significantly, 0.024 and 0.028, which increases the bond angle between the H_2O molecules from 103.749 to 104.683°. In both the —C═O and −O−R sites, O_S has a high electronegativity and easily gains electrons, and H_{w1} involved in the bond formation easily loses electrons, resulting in an increase in the O_S charge by 0.043 and 0.031 in —C═O and −O−R, respectively; however, the bond length elongation is not evident in —C═O and −O−R , both being 0.007 Å. The bond angle of the H_2O molecule in the H_2O/Ph—C═O adsorption configuration changes from 103.749 to 104.277°, whereas in the H_2O/Ph−O−R adsorption configuration, the bond angle of the H_2O molecule decreases from 103.749 to 102.946° due to the charge attraction of O_S to H_{W2}.

As listed in Table 6, for the CO_2 molecule in the Ph−COOH, Ph−OH, Ph—C═O, and Ph−O−R stable adsorption configurations, the O atoms in the OFGs all gain electrons, −0.011, −0.017, −0.01, and −0.01 e, respectively, and the C atoms in CO_2 all lose electrons, 0.016, 0.026, 0.02, and 0.02 e, while the two O atoms of CO_2 gain −0.012, −0.027, −0.024, and − 0.016 electrons, respectively. Figure 4e−h shows that the electron density difference diagrams are consistent with the results of the Mulliken atomic charge analysis. As shown in Table 7, the charge transfer is less when the CH_4 molecule is adsorbed by different OFGs, and the center C atoms of the CH_4 molecule all gain electrons, −0.028, −0.012, −0.009, and −0.009 e; the H atoms in the CH_4 molecule all lose electrons; and the charges of the atoms in the different OFGs do not change significantly. The same consistency can be observed even in Figure 4i−l.

Combining the adsorption energy and charge analysis of the H_2O, CO_2, and CH_4 molecules on different OFGs, it can be concluded that, the stronger the adsorption stability of different small molecules on the coal model surface for each OFG, the more evident the charge transfer between the group atoms, and the order of the adsorption stability of the small molecules on each OFG is H_2O > CO_2 > CH_4.

4. CONCLUSIONS

(1) The results of the PDOS and Mulliken bond layout analysis showed that H 1s orbitals and O 2p orbitals

https://doi.org/10.1021/acsomega.2c01278
ACS Omega 2022, 7, 17330−17338

interact to form hydrogen bonds. The average bond lengths of the H_2O molecules forming hydrogen bonds with −COOH, −OH, —C═O, and −O−R groups were 1.781, 1.841, 1.877, and 2.048 Å, respectively. Combining the numerical magnitude of the Mulliken bond layout, the delocalization of H 1s in PDOS, and the adsorption energy between the H_2O molecules and different OFGs, the order of the bond strength between the H_2O molecules and OFGs was found to be Ph−COOH > Ph−OH > Ph—C═O > Ph−O−R.

(2) The results of the adsorption energy calculations for the different molecules confirmed the interaction between the H_2O molecules and different OFGs via hydrogen bonding; hence, the adsorption stability of the H_2O molecules for each OFG was higher than those of the CO_2 and CH_4 molecules. The adsorption stability of the H_2O molecules for Ph−COOH was greater than that for the other OFGs because of the formation of two hydrogen bonds between the H_2O molecules and −COOH. Similarly, the adsorption stability of the CO_2 and CH_4 molecules for Ph−COOH was greater than that for the other OFGs.

(3) The results of the Mulliken charge layout and electron density difference analysis of the different molecules showed that after the adsorption of the H_2O molecules by the different OFGs, the O atoms in the OFGs easily gain electrons and that the H atoms involved in bonding with the H_2O molecules easily lose electrons, resulting in different degrees of elongation of the bond between the OFGs and H_2O molecules; the most evident elongation was of the O−H bonds in the −COOH groups at 0.032 Å. The difference in the adsorption configuration led to an increase in the bond angle of the H_2O molecule in the −COOH, −OH, and —C═O groups and a decrease in the case of the −O−R group. After the adsorption of the CO_2 molecules by different OFGs, all the O atoms in the OFG gained electrons, and all the C atoms in the CO_2 molecules lost electrons. After the adsorption of the CH_4 molecules by different OFGs, all the C atoms at the center of the CH_4 molecules gained electrons, while all the H atoms in the CH_4 molecules lost electrons. The electron gained and lost by the different molecules were consistent with the electron density difference diagrams.

(4) OFGs are important factors affecting gas adsorption; the adsorption stability of different small molecules for each OFG was found to be H_2O > CO_2 > CH_4, indicating that H_2O molecules have the highest adsorption capacity and that injecting water into the coal seam can improve the CBM yield; the adsorption effect of H_2O was better than that of CO_2, which can help accelerate the recovery of coal seam gases.

AUTHOR INFORMATION

Corresponding Author

Xiaoqing Liu − *College of Safety Science and Engineering, Liaoning Technical University, Fuxin 123000, China; Key Laboratory of Mine Power Disaster and Prevention of Ministry of Education, Huludao 125105 Liaoning, China;* orcid.org/0000-0002-3359-1260; Email: LXQab161616@163.com

Author

Dan Zhao − *College of Safety Science and Engineering, Liaoning Technical University, Fuxin 123000, China; Key Laboratory of Mine Power Disaster and Prevention of Ministry of Education, Huludao 125105 Liaoning, China*

Complete contact information is available at: https://pubs.acs.org/10.1021/acsomega.2c01278

Notes

The authors declare no competing financial interest.

ACKNOWLEDGMENTS

This work was supported by the Liaoning Provincial Department of Education Project (LJ2019JL025). The authors would like to thank all the reviewers who participated in the review, as well as MJEditor (www.mjeditor.com) for providing English editing services during the preparation of this manuscript.

REFERENCES

(1) Yu, H.; Zhou, L.; Guo, W.; Cheng, J.; Hu, Q. Predictions of the adsorption equilibrium of methane/carbon dioxide binary gas on coals using Langmuir and ideal adsorbed solution theory under feed gas conditions. *Int. J. Coal Geol.* **2008**, *73*, 115−129.

(2) Salmachi, A.; Haghighi, M. Feasibility Study of Thermally Enhanced Gas Recovery of Coal Seam Gas Reservoirs Using Geothermal Resources. *Energy Fuels* **2012**, *26*, 5048−5059.

(3) Deng, J.; Chu, W.; Wang, B.; Yang, W.; Zhao, X. S. Mesoporous Ni/$Ce_{1-x}Ni_xO_{2-y}$ heterostructure as an efficient catalyst for converting greenhouse gas to H_2 and syngas. *Catal. Sci. Technol.* **2016**, *6*, 851−862.

(4) Hu, J.; Guo, Z.; Chu, W.; Li, L.; Lin, T. Carbon dioxide catalytic conversion to nano carbon material on the iron−nickel catalysts using CVD-IP method. *J. Energy Chem.* **2015**, *24*, 620−625.

(5) Deng, J.; Cai, M.; Sun, W.; Liao, X.; Chu, W.; Zhao, X. S. Oxidative Methane Reforming with an Intelligent Catalyst: Sintering-Tolerant Supported Nickel Nanoparticles. *ChemSusChem* **2013**, *6*, 2061−2065.

(6) Zhang, D.-F.; Cui, Y.-J.; Liu, B.; Li, S.-G.; Song, W.-L.; Lin, W.-G. Supercritical Pure Methane and CO_2 Adsorption on Various Rank Coals of China: Experiments and Modeling. *Energy Fuels* **2011**, *25*, 1891−1899.

(7) Yang, X.; Wang, G.; Zhang, J.; Ren, T. The influence of sorption pressure on gas diffusion in coal particles: An experimental study. *Processes* **2019**, *7*, 219.

(8) Liu, Y.; Zhu, Y.; Liu, S.; Li, W.; Tang, X. Temperature effect on gas adsorption capacity in different sized pores of coal: experiment and numerical modeling. *J. Pet. Sci. Eng.* **2018**, *165*, 821−830.

(9) Müller, E. A.; Gubbins, K. E. Molecular simulation study of hydrophilic and hydrophobic behavior of activated carbon surfaces. *Carbon* **1998**, *36*, 1433−1438.

(10) Müller, E. A.; Rull, L. F.; Vega, L. F.; Gubbins, K. E. Adsorption of water on activated carbons: A molecular simulation study. *J. Phys. Chem.* **1996**, *100*, 1189−1196.

(11) Müller, E. A.; Hung, F. R.; Gubbins, K. E. Adsorption of water vapor methane mixtures on activated carbons. *Langmuir* **2000**, *16*, 5418−5424.

(12) Liu, H.; Song, D.; He, X. Effect of coalification on microsurface structure characteristics of coal. *J. China Saf. Sci.* **2020**, *30*, 121−127.

(13) Mathews, J. P.; van Duin, A. C. T.; Chaffee, A. L. The utility of coal molecular models. *Fuel Process. Technol.* **2011**, *92*, 718−728.

(14) Haenel, M. W. Recent progress in coal structure research. *Fuel* **1992**, *71*, 1211−1223.

(15) Nie, B.; Liu, X.; Yang, L.; Meng, J.; Li, X. Pore structure characterization of different rank coals using gas adsorption and scanning electron microscopy. *Fuel* **2015**, *158*, 908−917.

(16) Chen, S.; Tao, S.; Tang, D.; Xu, H.; Li, S.; Zhao, J.; Jiang, Q.; Yang, H. Pore structure characterization of different rank coals using N_2 and CO_2 adsorption and its effect on CH_4 adsorption capacity: a case in Panguan syncline, western Guizhou, China. *Energy Fuels* **2017**, *31*, 6034−6044.
(17) Levy, J. H.; Day, S. J.; Killingley, J. S. Methane capacities of Bowen Basin coals related to coal properties. *Fuel* **1997**, *76*, 813−819.
(18) Czerw, K. Methane and carbon dioxide sorption/desorption on bituminous coal—Experiments on cubicoid sample cut from the primal coal lump. *Int. J. Coal Geol.* **2011**, *85*, 72−77.
(19) Liu, L.; Jia, H. Finding the optimal social trust path in large scale wireless sensor networks. *IEICE Commun. Express* **2013**, *2*, 294−299.
(20) Zhang, J.; Liu, K.; Clennell, M. B.; Dewhurst, D. N.; Pervukhina, M. Molecular simulation of CO_2/CH_4 competitive adsorption and induced coal swelling. *Fuel* **2015**, *160*, 309−317.
(21) Zhao, Y.; Feng, Y.; Zhang, X. Molecular simulation of CO_2/CH_4 self and transport diffusion coefficients in coal. *Fuel* **2016**, *165*, 19−27.
(22) Hu, H.; Li, X.; Fang, Z.; Wei, N.; Li, Q. Small-molecule gas sorption and diffusion in coal: Molecular simulation. *Energy* **2010**, *35*, 2939−2944.
(23) Xia, Y.; Yang, Z.; Zhang, R.; Xing, Y.; Gui, X. Enhancement of the surface hydrophobicity of low-rank coal by adsorbing DTAB: An experimental and molecular dynamics simulation study. *Fuel* **2019**, *239*, 145−152.
(24) Huo, Y.; Zhu, H.; He, X.; Fang, S.; Wang, W. Quantum chemical calculation of the effects of H_2O on oxygen functional groups during coal spontaneous combustion. *ACS Omega* **2021**, *6*, 25594−25607.
(25) Wang, C.; Xing, Y.; Xia, Y.; Zhang, R.; Wang, S.; Shi, K.; Tan, J.; Gui, X. Investigation of interactions between oxygen-containing groups and water molecules on coal surfaces using density functional theory. *Fuel* **2021**, *287*, 119556.
(26) Xiang, J.; Zeng, F.; Liang, H.; Li, B.; Song, X. Molecular simulation of the $CH_4/CO_2/H_2O$ adsorption onto the molecular structure of coal. *Sci. China Earth Sci.* **2014**, *57*, 1749−1759.
(27) Xu, H.; Chu, W.; Huang, X.; Sun, W.; Jiang, C.; Liu, Z. CO_2 adsorption-assisted CH_4 desorption on carbon models of coal surface: A DFT study. *Appl. Surf. Sci.* **2016**, *375*, 196−206.
(28) Zhou, Y.; Sun, W.; Chu, W.; Liu, X.; Jing, F.; Xue, Y. Theoretical insight into the enhanced CH_4 desorption via H_2O adsorption on different rank coal surfaces. *J. Energy Chem.* **2016**, *25*, 677−682.
(29) Yu, S.; Bo, J.; Wu, L. Molecular simulation of $CH_4/CO_2/H_2O$ competitive adsorption on low rank coal vitrinite. *Phys. Chem. Chem. Phys.* **2017**, *19*, 17773−17788.
(30) Gensterblum, Y.; Busch, A.; Krooss, B. M. Molecular concept and experimental evidence of competitive adsorption of H_2O, CO_2 and CH_4 on organic material. *Fuel* **2014**, *115*, 581−588.
(31) Mosher, K.; He, J.; Liu, Y.; Rupp, E.; Wilcox, J. Molecular simulation of methane adsorption in micro- and mesoporous carbons with applications to coal and gas shale systems. *Int. J. Coal Geol.* **2013**, *109-110*, 36−44.
(32) Hao, S.; Wen, J.; Yu, X.; Chu, W. Effect of the surface oxygen groups on methane adsorption on coals. *Appl. Surf. Sci.* **2013**, *264*, 433−442.
(33) Qiu, N.-X.; Xue, Y.; Guo, Y.; Sun, W.-J.; Chu, W. Adsorption of methane on carbon models of coal surface studied by the density functional theory including dispersion correction (DFT-D3). *Comput. Theor. Chem.* **2012**, *992*, 37−47.
(34) Perdew, J. P.; Burke, K.; Ernzerhof, M. Generalized gradient approximation made simple. *Phys. Rev. Lett.* **1996**, *77*, 3865−3868.
(35) Chen, J.; Min, F.; Liu, L.; Peng, C. DFT calculations of different amine /ammonium cations adsorption on kaolinite (001) surface. *J. China Coal Soc.* **2016**, *41*, 3115−3121.
(36) Han, Y.; Liu, W.; Chen, J. Adsorption mechanism of hydroxyl calcium on two kaolinite (001) surface. *J. China Coal Soc.* **2016**, *41*, 743−750.
(37) Segall, M. D.; Lindan, P. J. D.; Probert, M. J.; Pickard, C. J.; Hasnip, P. J.; Clark, S. J.; Payne, M. C. First-principles simulation: ideas, illustrations and the CASTEP code. *J. Phys.: Condens. Matter* **2002**, *14*, 2717−2744.
(38) Vanderbilt, D. Soft self-consistent pseudopotentials in a generalized eigenvalue formalism. *Phys. Rev. B* **1990**, *41*, 7892−7895.
(39) Gao, Z.; Ding, Y. DFT study of CO_2 and H_2O co-adsorption on carbon models of coal surface. *J. Mol. Model.* **2017**, *23*, 187.
(40) Xia, Y.; Liu, X.; Liu, S. Adsorption mechanism of water molecules onto oxygen-containing functional groups of lignite. *Coal Convers.* **2016**, *39*, 1−5.
(41) Gao, Z.; Ding, Y.; Yang, W.; Han, W. DFT study of water adsorption on lignite molecule surface. *J. Mol. Model.* **2017**, *23*, 27.
(42) Gao, Z.; Li, M.; Sun, Y.; Zhao, L. Adsorption mechanism of lignite and water molecules. *J. China Coal Soc.* **2017**, *42*, 505−511.
(43) Cheng, G.; Li, Y.; Zhang, M.; Cao, Y. Simulation of the adsorption behavior of $CO_2/N_2/O_2$ and H_2O molecules in lignite. *J. China Coal Soc.* **2021**.
(44) Gao, Z.; Ma, C.; lv, G.; Li, A.; Li, X.; Liu, X.; Yang, W. Car-Parrinello molecular dynamics study on the interaction between lignite and water molecules. *Fuel* **2019**, *258*, 116189.

https://doi.org/10.1021/acsomega.2c01278
ACS Omega 2022, 7, 17330−17338